INVESTIGATIONS OF TURBULENCE STATISTICS IN THE LABORATORY MODEL OF AN ATMOSPHERIC CLOUD

P. M. Korczyk*,T. A. Kowalewski* S. P. Malinowski**
* IPPT PAN, Department of Mechanics & Physics of Fluids, Warszawa, Poland
**Warsaw University, Institute of Geophysics, Warszawa, Poland

ABSTRACT

Mixing of air containing small water droplets is investigated in the laboratory model to elucidate smallest scales of air entrainment and mixing in real clouds. Particle Image Velocimetry (PIV) is applied to evaluate turbulent characteristics of the flow field generated in the cloud chamber by buoyancy of the introduced mist. It permits to investigate dynamics of the process for scales from 0.07 mm to few centimeters, characteristic for a real cloud microphysics. Three velocity components retrieved in the vertical cross-section through the chamber interior indicate anisotropy of small-scale turbulent motions, with the preferred vertical direction. This result confirms earlier numerical studies, indicating, that evaporation of cloud droplets at the cloud-clear air interface may substantially influence the small-scale turbulence in clouds.

1 INTRODUCTION

The so called "warm rain initiation problem" attracts attention of cloud physicists, turbulence researchers, engineers and meteorologists. It is still uncertain which mechanism is responsible for the formation of drizzle and rain (precipitation) drops. Papers concerning the impact of high-Reynolds-number turbulence on spatial distribution of cloud droplets, their diffusional growth, collisions, and coalescence are published at high rate. Our understanding of particle motion in turbulent flows is based on both theoretical and experimental studies [1] [2] [3]. In particular, these works show that small-scale turbulence, i.e. with spatial scales comparable with the Kolmogorov length scale, may influence the spatial distribution of droplets and yield non-Poisson statistics. Due to the inertia, the relative velocity between falling droplets depends not only on their terminal velocity and collision efficiency increases. As a consequence, particles tend to diverge out of regions of high vorticity nad converge preferentially in regions of low vorticity. Regions of much higher and lower concentration than predicted from Poisson spatial distribution can develop. Direct visual evidence of preferential concentration has been obtained in several laboratory experiments, even for very slow convective flow of viscous liquid in a cube-shaped cavity [4]. On the other hand, droplets can mechanically and thermodynamically (latent heat release) influence the small-scale flow in a complex manner. The flow in regions of mixing may not be isotropic because of the negative buoyancy produced by droplet evaporation. Hence, it is expected that the -5/3 power law observed in cumulus clouds at scales between 15 and 200 m also extends down to the smaller scales in the cloud core [5].

Unfortunately, due to the experimental constrains, properties of the cloud turbulence at scales relevant for the interactions between droplets and the air flow have never been documented. Recently Siebert et al. [6] were able to study turbulent velocities at scales down to 20 cm. Such a scale is still

about two orders of magnitude larger than a typical distance between cloud droplets, which, coincidentally, is also the Kolmogorov microscale for typical levels of cloud turbulence. It follows that far-reaching assumptions have to be made in order to study interaction between cloud dynamics, thermodynamics, and microphysics. Usually it is assumed, that cloud turbulence is generated at large scales (100m or more), and it cascades through the inertial range of turbulent eddies down to the Kolmogorov microscale, where it is dissipated. At the smallest scales turbulent velocities are usually assumed to be isotropic and they are described by statistical distributions based on laboratory/wind tunnel/atmospheric boundary layer measurements or direct numerical simulation (DNS). It is also assumed that temperature and humidity are passive scalars, i.e. they do not influence small-scale dynamics through the buoyancy effects [7] [8] [9]. In the following we show that these assumptions are not always fulfilled. We present laboratory cloud chamber experiments with turbulent mixing between cloudy air and unsaturated clear air at scales down to a fraction of a centimeter. It appears that at these scales turbulence is substantially anisotropic due to the action of buoyancy forces resulting from evaporation of cloud droplets. Recently several attempts to simulate directly the interface microscale mixing are reported [10] [11] [12]. DNS simulations performed to mimic laboratory experiment reported by Malinowski et al. [13] evidently confirm that buoyancy forces resulting from evaporation may substantially modify smallest scale of turbulence.

2 EXPERIMENT

2.1 Experimental setup

In the following experiment we adopt cloud chamber previously constructed to analyze spatial distribution of droplets [14] [15]. The flow of water mist is generated in a glass-walled chamber of size $1x1x1.8m^3$ (Fig. 1). On the top of this chamber a smaller box is located. This box is filled with the water mist using standard ultrasound humidifier. Liquid water content increases density of the mixture collected in the upper box. Once the box is completely saturated with the mixture a circular opening of 10cm diameter, connecting it with the cloud chamber, is abruptly unblocked. The cloudy plume of the small negative buoyancy smoothly enters the chamber with the velocity of approximately 10 cm s^{-1}. The plum interacts with a quiescent air stimulating turbulent mixing of cloud droplets with the unsaturated air. It descends slowly when mixing with the environment, forming turbulent filaments of dry and cloudy air. This process is visualized in the planar cross-section of the chamber using the laser light sheet technique (comp. Fig. 2). For this purpose tandem of two pulsed lasers (Nd:Yag, wavelength 532nm) is used. It permits to illuminate interior of the chamber with pairs of 5ns light pulses of 36mJ energy and repetition rate of 12Hz. An optical system with cylindrical lenses provides 1-mm thick light sheet of about 15cm width. Images of the cloud are observed from the perpendicular direction. For the recording, one or two high resolution CCD cameras (PCO Sensi-Cam) are used in conjunction with a PC Pentium 4/HT computer and a frame grabber. The system allows for storing up to 200 pairs of 1280x1024pixels 12bit images in the computer RAM at a rate of 4.5Hz. The time interval between two laser pulses can be adjusted from minimum delay of 200ns in order to select the appropriate delay between the images. Usually for typical experiments it is of order of 1ms. During experimental runs separate equipment is used to continuously monitor temperature in the filling box and in the cloud chamber (4 measuring points). Atmospheric air pressure, temperature and humidity are monitored as well. Liquid water content and droplets size distribution is estimated by taking samples of the mixture during separate control experiments. A typical image (negative) of the cloud observed in the chamber is presented in Fig. 2. The image area covers about $7x4.5cm^2$ in the center of

the chamber. Inspection of collected images reveals a very fine filamented structure created in the process of turbulent mixing of cloudy plume with unsaturated environment. One pixel in the image corresponds to about 1mm x 55µm x 55µm volume of air. Bright pixels indicate elementary volumes occupied by droplets. However, due to the Mie scattering properties, there is no simple relation between between the brightness of the pixel and concentration of droplets. Identification of patterns in the two consecutive images separated by a known time interval allows for determination of two components of motion of the patterns in the plane of the image [16]. This technique, widely adopted in experimental fluid dynamics, is known as Particle Image Velocimetry (PIV) [17].
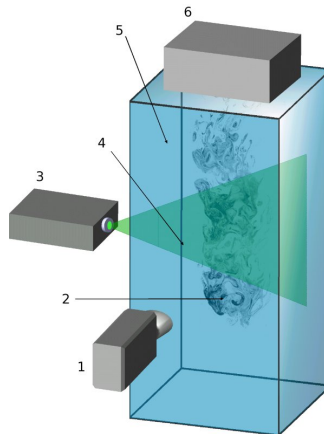

Fig 1: The experimental setup: 1) CCD camera 2) cloud during mixing, 3) double-pulse laser, 4) laser sheet, 5) cloud chamber, 6) small chamber with the droplet generator inside

Fig 2: The negative of the cloud image from the experimental chamber showing small-scale structures created in a process of cloud-clear air mixing. Imaged area corresponds to 7cm x 4.5cm in physical space.

2.2 Particle Image Velocimetry

Three PIV setups are applied to evaluate velocity field in the cloud model. 2C PIV is used to obtain two component velocity field from pairs of images recorded by one camera, arranged perpendicularly to the laser light sheet. In 3C stereo PIV method two cameras are used, recording images from different

angles relative to the axis perpendicular to the laser light sheet. In this case data from two pairs of images are combined to obtain all three components of the velocity field. Both methods are used to retrieve spatial fluctuations of the velocity field. In the third imaging setup, a 5W CW Argon laser and high speed CCD camera (PCO HS1200) are used to record long time sequences of images at about 1kHz rate. It allows us to observe changes of the velocity field in time and to retrieve its temporal fluctuations in the plane.

2.4.1 2C PIV evaluation methodology

Droplets visualized in the chamber differ from typical tracers used for seeding the flow in the standard PIV approach. Cloud droplets are not monodisperse and they are non-uniformly distributed, occupying only part of the PIV image in several distinct filaments. Standard PIV algorithms based on fixed interrogation windows are optimized for the more uniform distribution of markers in the flow. Such algorithms, initially adopted to retrieve turbulent velocity fields in the chamber, produced many artifacts. Hence, in order to improve PIV evaluation a new multi-scale algorithm for image processing was developed. This algorithm resembles other multi-scale algorithm described in the literature [17], but is optimized for this particular experimental application.

Consider a pair of images collected at a given time interval. Each image is represented by a matrix of the size of 1280x1024, equal to the size of the CCD element in the camera. Brightness of each pixel is represented by the 12-bit integer element of the matrix. In order to evaluate displacement of a droplet pattern at position *(x,y)* a square section of the matrix from the first exposure centered at this position is taken. Then the search of the most similar square sample of the same size in the interrogation area embedded inside the second exposure is being performed. The size of the interrogation area depends on the expected greatest displacement and on the size of the sample. For an interrogation window $\boldsymbol{S}$ of size *MxM* and for an interrogation area $\boldsymbol{A}$ of size *LxL* the evaluation function used to search the most similar sample is defined by the following formula:

$$\phi(m,n)=\sum_{i=1}^{M}\sum_{j=1}^{M}[\boldsymbol{S}(i,j)-\langle\boldsymbol{S}\rangle][\boldsymbol{A}(i+m,j+n)-\langle\boldsymbol{A}\rangle_{m,n}] \tag{1}$$

where:

$$\langle\boldsymbol{S}\rangle=\frac{1}{M^2}\sum_{i=1}^{M}\sum_{j=1}^{M}\boldsymbol{S}(i,j), \qquad \langle\boldsymbol{A}\rangle_{m,n}=\frac{1}{M^2}\sum_{i=1}^{M}\sum_{j=1}^{M}\boldsymbol{A}(i+m,j+n) \tag{2}$$

For $m\in[0,L-M]$ $\quad n\in[0,L-M]$ the evaluation function can be written as:

$$\phi(m,n)=\sum_{i=1}^{M}\sum_{j=1}^{M}\boldsymbol{S}(i,j)\boldsymbol{A}(i+m,j+n)-M^2\langle\boldsymbol{S}\rangle\langle\boldsymbol{A}\rangle_{m,n} \tag{3}$$

Maximum of *Φ(m,n)* corresponds to highest similarity between samples from both exposures, from which displacement of the ensemble of droplets contained in $\boldsymbol{S}$ is evaluated. Figure 3 illustrates an example of an interrogation window, interrogation area and resulting evaluated function *Φ(m,n)*.

The particular form of *Φ(m,n)* was selected from many possible choices [18] in order to minimize possible errors of the displacement retrievals. The additional advantage of *Φ(m,n)* is that it can be efficiently calculated with use of the FFT algorithm.

In standard PIV algorithms a proper choice of the interrogation window is a significant technical problem [18]. In order to overcome this difficulty, the algorithm successively decreases windows size, sampling smaller and smaller area. In a first step it looks for the displacement in the whole image in order to remove the bulk motion of the plume. At the next step the size of the sample is reduced and

the displacement vector evaluated earlier determines the position of the interrogation area. In this way the displacement is corrected. This algorithm is repeated few times with the decreasing size of the sample, giving successive corrections for the velocity in smaller and smaller scales. After such sequence of operations two components of turbulent velocity are evaluated for small patterns. In addition, to improve accuracy in presence of high gradients of velocities and pixels brightness variations at each iteration image deformations algorithm is applied. This technique is widely used for adopting interrogation widows to local velocity gradients [19]. Here, calculated velocity field is used to deform the whole first image from the pair. After that it becomes more similar to the second image and in the next step the field of displacement is evaluated for a pair consisting of the first deformed image and the second original one. In such a way the correction of the field of displacement from the previous step can be evaluated. This procedure is repeated several times until the subsequent corrections are efficiently small.
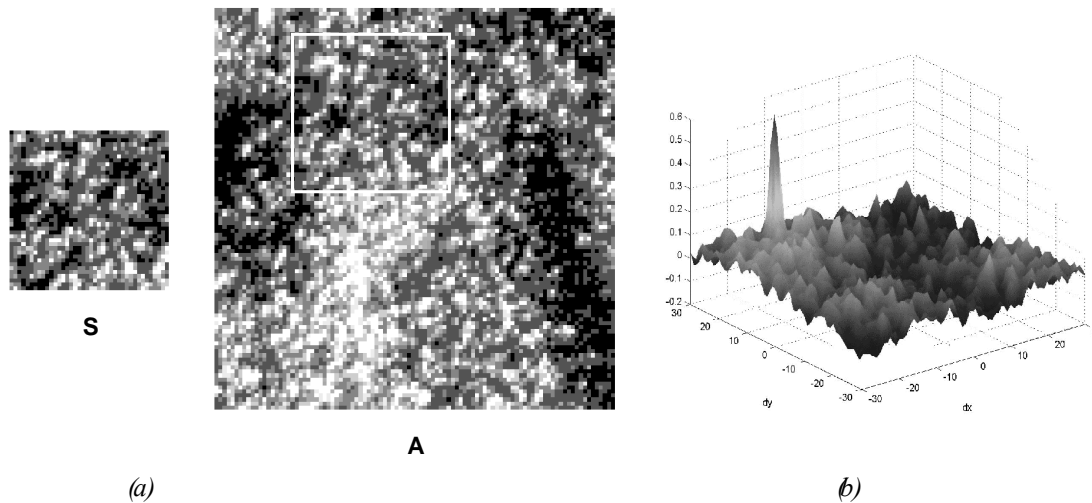

(a)   (b)

Fig 3: (a) - An example of image section S (40×40 pixels) for the first exposure and the corresponding interrogation area A (100×100 pixels) of the second exposure extracted from the pair of images. The most similar part is highlighted. *(b)* - an example of the evaluation function Φ(m,n) obtained for the experimental data presented in *(a)*.

The obvious limitation of the method is that the retrieved velocity field is limited to the cloudy part of the imaged flow. In the regions with the clear air we do not have information of the turbulent motion. A suitable mask has been created for each scene to depict areas without droplets. This mask has been applied to further statistical analysis of the data. It should be remembered that results given below represent only those parts of the volume where concentration of droplets is sufficient to perform our PIV analysis. It must be underlined, that application of the PIV technique to the cloud droplets, which, due to inertia and gravity may move with respect to the airflow, causes problem in the interpretation. With the presented approach we do not detect the velocity of the air, but velocity of droplet patterns conveyed by the flow.

2.4.1 Stereo PIV evaluation

The stereo PIV system applied consists of two cameras observing the same area of the flow simultaneously. Each camera view the object from different angle, hence stereoscopic conditions are obtained. Stereo PIV is applied to retrieve all three velocity components for the plane defined by the laser light sheet. In our case two different 3C-PIV evaluation software were used. The first one is

commercial package VidPIV developed by GmbH ILA (Germany, http://www.ila.de). For the stereo system calibration it uses a special target consisting of several rows of precise markers placed on two parallel plates. The perspective properties of stereoscopic projection of images is reconstructed using known information about positions of markers in real 3D space, and positions of the same markers on 2D plane of image. The second 3C-PIV system applied is based on the Optical Flow methodology [20], extended to stereo images. The new 3C software developed by George Quenote uses only one calibration target and known geometry of the optical system. It automatically finds the target markers and evaluates calibration matrix necessary for further reconstruction of tracers displacement.

2.3 Droplets spectrum and liquid water content

In additional experimental runs droplets in the cloud plume are collected on the oil film covering microscopic glass sheet and immediately thereafter photographed with a CCD camera under the microscope. In order to estimate the droplets spectrum the software recognizing droplets in images and calculating their radius is applied. Fig. 4 shows result of the droplets size evaluation obtained from about 20 measurements. It clearly indicates non-uniformity of the cloud droplets size with a characteristic double-peak shape. Accuracy of droplet diameter measurements is quite good (3% error). However, it must be mentioned that despite short time (~10s) of a single measurement, we cannot exclude possible bias in droplets size due to the evaporation of the droplets on the microscope slit.
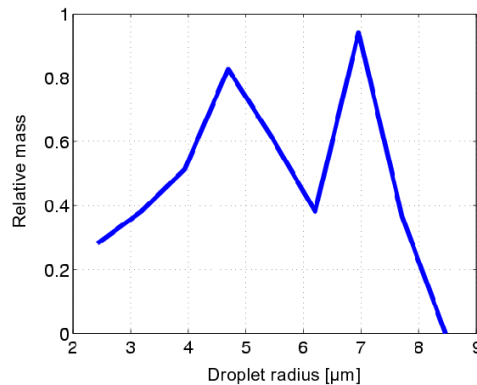

Fig 4: Spectrum of droplets.

Initial liquid water content (the ratio of mass of liquid water containing certain portion of air to the mass of this portion) of cloudy air is estimated in additional experiment. Well defined, 10 liter sample of saturated cloudy air entering main chamber is gravitationally sucked into a container. During this operation sucked air-water mixture passes through a cotton wool filter were droplets are trapped. Weight of the filter before and after the experiment allows us to evaluate mass of water droplets being sucked with the given portion of air. It was found that liquid water content in our experiments is typically about 20g/kg.

3 RESULTS

3.1 Energy dissipation rate and Kolmogorov length

The Kolmogorov phenomenological theory [21], formulated for fully developed homogeneous turbulence, appeared in several experimental studied to work well for small scales, typical for laboratory models. The two dimensional velocity fields obtained from the PIV measurements in the

cloud chamber give us possibility to estimate the Kolmogorov length (4). It is found that it varies in the narrow range form about 7.2 10^{-4} m to 7.8 10^{-4} m . The mean value of the Kolmogorov length obtained during our laboratory experiments is $7.6 \cdot 10^{-4}$m. It is typical for cumulus clouds in presence of weak convection [22]. It is interesting to note that the Kolmogorov length appears to depend on the relative humidity of air, i.e. initial humidity measured in the chamber before the plum with droplets is introduced.

$$\text{Kolmogorov length:} \quad \eta = \left(\frac{v^3}{\varepsilon}\right)^{1/4} \quad \text{- where } v \text{ is viscosity and } \varepsilon \text{ is energy dissipation rate.} \tag{4}$$
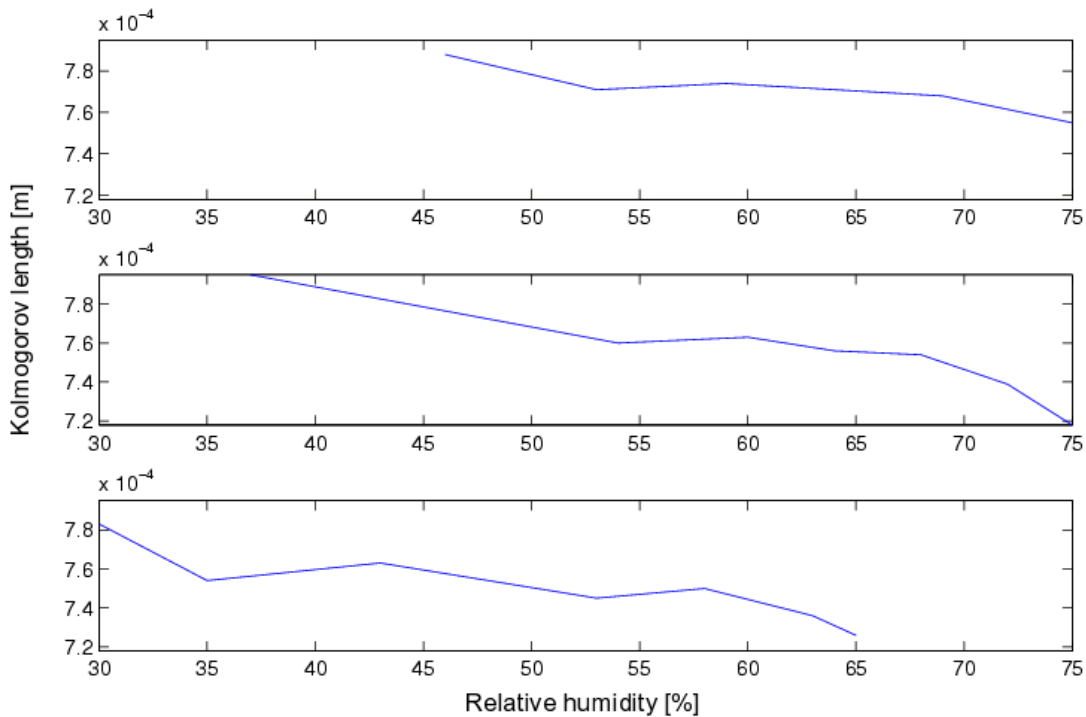

Fig 5: Experimental value of Kolmogorov length as a function of relative humidity. Each of charts corresponds to another experimental run.

Figure 5 presents variation of the evaluated Kolmogorov length in time for three different independent experimental runs. During each of these runs initial relative humidity inside the main chamber is increased. It becomes evident that the Kolmogorov length is systematically decreasing with the relative humidity, indicating that properties of the small scale turbulence may depend on efficiency of the droplets evaporation.

3.2 Statistics of velocity field

Three series of experiments with slightly varying thermodynamical conditions inside the chamber are performed. In each series, at least 500 pairs of frames (tens of thousands of vectors in each frame) are evaluated in order to retrieve properties of turbulent velocity fluctuations. Our analysis of stereo PIV data indicates that in horizontal plane velocity fluctuations are isotropic. Hence, in the following one horizontal component is presented. Combined statistics of turbulent velocity fluctuations in horizontal

(u') and vertical (w') directions are displayed in Fig. 6 and summarized in Table 1. Here, customary definition of standard deviation, skewness and kurtosis are used:

$$\sigma_u = \sqrt{\langle u'^2 \rangle} \quad , \qquad S_u = \frac{\langle (u')^3 \rangle}{\sigma_u^3} \quad , \qquad K_u = \frac{\langle (u')^4 \rangle}{\sigma_u^4} \quad . \tag{5}$$
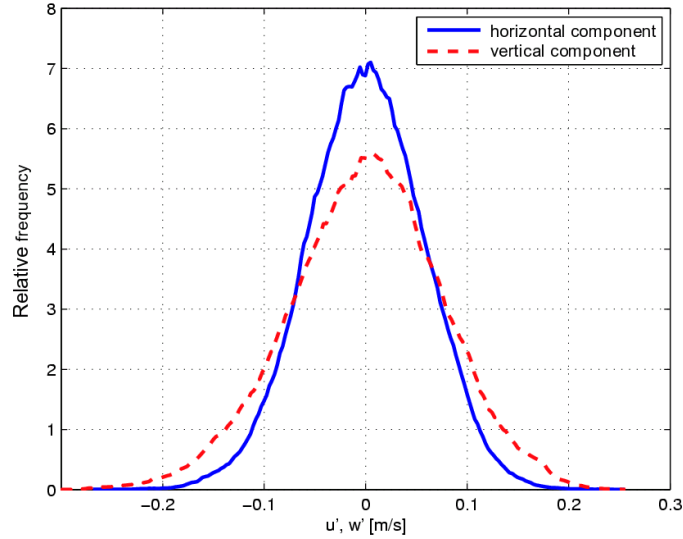

*Fig 6: D*istribution of horizontal (red) and vertical (blue) turbulent velocity fluctuations from three series of measurements.

TABLE 1. Distribution of horizontal (u') and vertical (w') turbulent velocity fluctuations for the experimental data shown in Fig. 6.

	Standard deviation [cm/s]	*Skewness*	*Kurtosis*
u'	5.4	-0.01	3.2
w'	8.0	-0.2	3.1

It is evident that the distribution of the vertical velocity fluctuations characterizes larger dispersion and it has longer tails than the distribution of horizontal velocity fluctuations. Calculated skewness and kurtosis indicate that both distributions are close to the Gaussian (normal). These results has been used to validate recent direct numerical simulations performed for similar conditions by Malinowski et al. [13]. It confirms strong influence of the buoyancy forces on the developed of turbulent fluctuations.

3.3 Structure functions

In order to evaluate the persistence of the turbulence, the second order structure function was calculated for the velocity flow in the small section of the cloud chamber, evaluating solely area covered by the imaging system (7cm x 4.5cm). The second order structure function appears useful to discriminate viscous and inertial range of the turbulent flow [23] [24]. The second order longitudinal structure function is a mean velocity increment between two points separated by *l,* projected onto the line of separation. Hence, we can introduce structure function for both *x* and *z* direction and obtain its variation for horizontal and vertical velocity components *u , w :*

$$S_u^{\parallel}(l) = \langle [u(x+l,z) - u(x,z)]^2 \rangle, \qquad (6)$$
$$S_w^{\parallel}(l) = \langle [w(x,z+l) - w(x,z)]^2 \rangle.$$
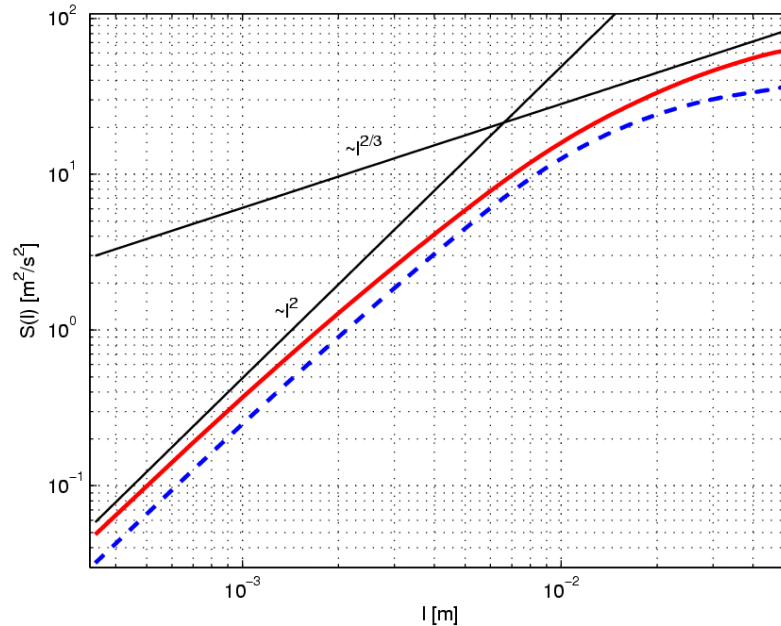

Fig 7: Second order longitudinal structure functions shown in log-log scale. Red solid line – vertical components. Blue dashed line – horizontal component. Straight lines indicate initial slope exponent (l^2) and asymptotic slope exponent ($l^{2/3}$)

Figure 7 clearly shows different behavior of the structure function for vertical and horizontal velocity components. Whereas initially both structure functions follow l^2 slope, characteristic for the dissipation range, at larger separations the inertial range $l^{2/3}$ behavior can be observed for the vertical velocity only. It indicates already mentioned anisotropy of the velocity field structures present for all scales observed in the laboratory experiments.

CONCLUSIONS

Small scale mixing of cloud with unsaturated environment is investigated in laboratory cloud chamber by means of Particle Image Velocimetry (PIV). The high spatial resolution of the experimental setup (0.07mm) allowed us to evaluate statistics of the turbulent flow field down to the Kolmogorov length. The results indicate that small-scale turbulence in such conditions is highly anisotropic with the preferred vertical direction. The present investigation indicates also that properties of turbulence in small scales is sensitive to the initial air humidity. Hence, obviously buoyancy forces resulting from evaporation of cloud droplets substantially influence smallest scales of turbulence. Typically, $\langle (u')^2 \rangle$ is about two times smaller than $\langle (w')^2 \rangle$. The probability distribution functions of w' are broader than those of u'. These results have been successfully used to validate numerical simulations (DNS) performed for a similar experimental configuration [13]. However, it is still uncertain to what extent infromation gained in the laboratory cloud can be applied to atmospheric systems. Hence, in situ measurements of turbulent velocity fluctuations from various types of clouds are necessary to validate common assumptions on small-scale cloud isotropy.

REFERENCES

1. Falkovich G, Gawedzki K and Vergassola M. Particles and fields in fluid turbulence. *Rev. Modern Phys.*, Vol. 73, pp 913-975, 2001.

2. Shaw RA. Particle-turbulence interactions in atmospheric clouds. *Annual Review of Fluid Mechanics*, Vol. 35, pp 183-227, 2003.

3. Ghosh S, Davila J, Hunt JCR, Srdic A, Fernando HJS., Jonas PR. How turbulence enhances coalescence of settling particles with applications to rain in clouds. *Proc. R. Soc. A*, Vol. 461, pp 3059-3088, 2005.

4. Yarin A, Kowalewski T A, Hiller WJ, Koch S. Distribution of particles suspended in 3D laminar convection flow. *Physics of Fluids*, Vol. 8, pp 1130-1140, 1996.

5. Vaillancourt PA, Yau MK. Review of particle-turbulence interactions and consequences for cloud physics. *Bull. Am. Meteorol. Soc.*, Vol. 81, pp 285–98, 2000.

6. Siebert H, Lehmann K and Wendish M. Observations of small-scale turbulence and energy dissipation rates in the cloud boundary layer. *J. Atmos. Sci.*, Vol. 63, pp 1451-1466, 2006.

7. Pinsky M and Khain AP. Turbulence effects on the collision kernel, Part 1: Formation of velocity deviations of drops falling within a turbulent three-dimensional flow. *Quart. J. Roy. Meteor. Soc.*, Vol. 123, pp 1517-1542, 1997.

8. Shaw RA, Walter CR, Lance RC and Johannes V. Preferential concentration of cloud droplets by turbulence: Effects on the early evolution of cumulus cloud droplet spectra. *J. Atmos. Sci.*, Vol. 55, pp 1965-1976, 1998.

9. Shaw RA and Oncley S P.. Acceleration intermittency and enhanced collision kernels in turbulent clouds. *Atmos. Res.*, Vol. 59-60, pp 77-87, 2001.

10. Vaillancourt PA, Yau MK and Bartello P, Grabowski WW. Microscopic Approach to Cloud Droplet Growth by Condensation. Part II: Turbulence, Clustering, and Condensational Growth. *J. Atmos. Sc.*, Vol. 59, pp 3421–3435, 2002.

11. Grabowski WW. MJO-like coherent structures: Sensitivity simulations using theCloud-Resolving Convection Parameterization (CRCP). *J. Atmos. Sci.*, Vol. 60, pp 847–864, 2003.

12. Andrejczuk M, Grabowski W, Malinowski SP and Smolarkiewicz PK. Numerical Simulation of Cloud-Clear Air Interfacial Mixing. *J. Atmos. Sci.*, Vol. 61, pp 1726–1739, 2004.

13. Malinowski SP and Andrejczuk M, Grabowski WW, Korczyk P, Kowalewski TA and Smolarkiewicz PK. Cloud-clear air interfacial mixing: anisotropy of turbulence generated by evaporation of liquid water. Laboratory observations and numerical modeling. *12th Conference on Cloud Physics*, Madison (WI, USA), 2006.

14. Malinowski SP, Zawadzki I, and Banat P. Laboratory observations of cloud-clear air mixing in small scales. *J. Atmos. Oceanic Technol.*, Vol. 15, pp 1060-1065, 1998.

15. Jaczewski A, Malinowski SP. Spatial distribution of cloud droplets in a turbulent cloud-chamber flow. *Quart. J. Roy Meteor. Soc.*, Vol. 131, pp 2047-2062, 2005.

16. Korczyk P, Malinowski SP, Kowalewski TA. Mixing of cloud and clear air in centimeter scales observed in laboratory by means of particle image velocimetry. *Atmos. Res.*, (in press), 2006.

17. Raffel M, Willert ChE and Kompenhans J. *Particle image velocimetry: a practical guide*. 3rd edition, Springer, 1998.

18. Gui L., W. Merzkirch. Generating arbitrarily sized interrogation windows for correlation-based analysis of particle image velocimetry recordings. *Exp. Fluids*, Vol. 24, pp 66-69, 1998.

19. Scarano F. Iterative image deformation methods in PIV. *Meas. Sci. Technol.*, Vol. 13, pp R1-R19, 2002.

20. Quenote G, Pakleza J, Kowalewski TA. Particle Image Velocimetry with Optical Flow. *Experiments in Fluids*, Vol. 25, pp 177-189, 1998.

21. Kolmogorow AN. Dissipation of energy under locally isotropic turbulence. *CR Acad. Sci. USSR*, Vol. 32, pp 16-18, 1941.

22. Pruppacher HR, Klett JD. *Microphysics of clouds and precipitation*. 1st edition, Kluwer, 1997.

23. Frish U. *Turbulence - The legacy of A. N. Kolmogorov*. 1st edition, Cambridge University Press, 1995.

24. Batchelor GK. Pressure fluctuations in isotropic turbulence. *Proc. Cambridge Phil. Soc.*, Vol. 47, pp 533-559, 1951.